Theory of amplification of eigenmode acoustic surface waves in thin bismuth films



1990 J. Phys.: Condens. Matter 2 5499

(http://iopscience.iop.org/0953-8984/2/25/003)

J. Phys.: Condens. Matter **2** (1990) 5499–5515. Printed in the UK

# Theory of amplification of eigenmode acoustic surface waves in thin bismuth films

Chhi-Chong Wu† and Jensan Tsai‡

† Institute of Electronics, National Chiao Tung University, Hsinchu, Taiwan, Republic of China

‡ Institute of Nuclear Science, National Tsing Hua University, Hsinchu, Taiwan, Republic of China

Received 15 November 1989, in final form 13 March 1990

**Abstract.** Amplification characteristics of eigenmode acoustic waves in thin bismuth films are investigated quantum-mechanically in the gigahertz frequency region. Numerical results show that the amplification coefficient for the P-SV mode (pressure wave–shear wave with vertical polarisation) oscillates with the frequency in the higher-frequency region, and these oscillations diminish as the temperature decreases. For the SV-P mode (shear wave with vertical polarisation–pressure wave), the amplification coefficient oscillates with the frequency in the higher-frequency region for the EP (ellipsoidal parabolic), ENP (ellipsoidal non-parabolic) and MNENP (modified non-ellipsoidal non-parabolic) models, but no oscillations can be observed for the NENP (non-ellipsoidal non-parabolic) model. These oscillations also diminish as the temperature decreases. No amplification can be observed for the SH mode (shear wave with horizontal polarisation) in thin bismuth films. For the TR mode (total reflection), no oscillations of the amplification coefficient can be observed, and this appears to be the same property as that for Rayleigh waves.

## 1. Introduction

Bismuth is a semimetal with highly anisotropic Fermi surfaces. Its constant-energy wavevector surfaces differ considerably from the simple spherical surfaces of the degenerate electron gas. Some early work demonstrated that the Fermi surface for electrons in bismuth can be satisfactorily described by the ellipsoidal parabolic (EP) model (Shoenberg 1957). For this EP model, the relation between the energy $E$ and the momentum $\boldsymbol{p} = (p_x, p_y, p_z)$ of conduction electrons can be expressed as

$$E = p_x^2/2m_1 + p_y^2/2m_2 + p_z^2/2m_3 \tag{1a}$$

where $m_1$, $m_2$ and $m_3$ are the effective masses of electrons along $x$, $y$ and $z$ axes, respectively. From theoretical calculations (Cohen 1961) and experimental results (Koch and Jensen 1969, Dinger and Lawson 1970, 1971, 1973), it was pointed out that the energy band of bismuth follows the Cohen non-ellipsoidal non-parabolic (NENP) model. However, the magneto-optical results (Maltz and Dresselhaus 1970, Vecchi *et al* 1976) and the longitudinal magneto-striction (Michenaud *et al* 1981, 1982) supported the Lax ellipsoidal non-parabolic (ENP) model (Lax 1958). The relation between the

0953-8984/90/255499 + 17 $03.50  

energy and the momentum of conduction electrons for the ENP model can be expressed as

$$E(1 + E/E_g) = p_x^2/2m_1 + p_y^2/2m_2 + p_z^2/2m_3 \tag{1b}$$

where $E_g$ is the energy gap between the conduction and valence bands. For the NENP model, the energy–momentum relation of electrons can be expressed as

$$E(1 + E/E_g) = p_x^2/2m_1 + p_y^2[1 + E(1 - m_2/m_2')/E_g]/2m_2 + p_z^2/2m_3 + p_y^4/4m_2m_2' E_g. \tag{1c}$$

From experimental results (Dinger and Lawson 1970, 1971, 1973), it was indicated that the difference between $m_2$ and $m_2'$ is quite small, i.e. $m_2 \simeq m_2'$. McClure and Choi (1977) presented a new energy-band model for bismuth electrons, which is more general than those currently in use. They showed that it can fit the data for a large number of magneto-oscillatory and resonance experiments. This new energy-band model is called the McClure–Choi modified non-ellipsoidal non-parabolic (MNENP) model. The relation between the energy and momentum of conduction electrons for this model can be expressed as

$$E(1 + E/E_g) = p_x^2/2m_1 + p_y^2[1 + E(1 - m_2/m_2')/E_g]/2m_2 + p_z^2/2m_3 + p_y^4/4m_2m_2' E_g - p_x^2p_y^2/4m_1m_2E_g - p_y^2p_z^2/4m_2m_3E_g. \tag{1d}$$

The main difference between the MNENP and NENP models is that there are two extra terms, $-p_x^2p_y^2/4m_1m_2E_g$ and $-p_y^2p_z^2/4m_2m_3E_g$, in equation (1*d*).

The interaction between acoustic waves and conduction electrons in solids provides a useful tool to investigate the electronic band structure of matter. Acoustic waves can be propagated along the boundary of an elastic half-space (Ezawa 1971), the amplitude of which falls off rapidly as one goes away from the surface. Such elastic excitations are called Rayleigh waves (Grishin and Kaner 1972). In an elastic medium with a stress-free plane boundary, acoustic waves can propagate along the boundary of an elastic half-space and are then reflected on the boundary (Ezawa 1971). Therefore, there exist four different kinds of acoustic waves other than the Rayleigh wave. They are referred to as the P-SV (pressure wave-shear wave with vertical polarisation) mode wave, the SV-P (shear wave with vertical polarisation–pressure wave) mode wave, the SH (shear wave with horizontal polarisation) mode wave and the TR (total reflection) mode wave. These four eigenmode waves are shown in figures 1(*a*)–(*d*).

If a longitudinal pressure wave propagating in a medium is incident upon the stress-free boundary surface, a longitudinal P wave and a SV wave are reflected from the surface. This is called the P-SV mode, as shown in figure 1(*a*). In this case, the angle of incidence and reflection for the P wave are equal to each other, while the angle of reflection $\theta_{SV}$ for the SV wave is smaller than the angle of reflection $\theta_P$ for the P wave because the SV wave travels more slowly than the P wave. When a SV wave propagating in the medium is incident upon the stress-free boundary surface with a small angle of incidence, a SV wave and a P wave come out as the reflected waves from the surface, but this P wave cannot be totally reflected from the surface. This is called the SV-P mode, as shown in figure 1(*b*). If we project the SH wave on the stress-free boundary surface, the SH wave is reflected from the surface with the same angle of reflection and incidence (figure 1(*c*)). In this case, no wave other than the SH wave appears as the reflected wave, because the displacements of the SH wave are parallel to the surface. Finally, if a SV wave propagating in a medium is incident upon the stress-free boundary surface, a SV wave and a P wave

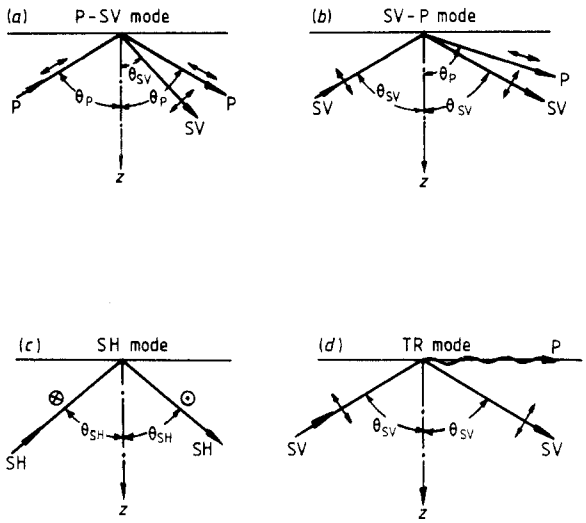


**Figure 1.** (*a*) P-SV mode consists of an incident P wave with angle of incidence $\theta_P$ and reflected P wave with angle of reflection $\theta_P$ and SV wave with angle of reflection $\theta_{SV}$. (*b*) SV-P mode consists of an incident SV wave and reflected SV and P waves. (*c*) In SH mode, both incident and reflected waves are SH waves with the angle of incidence being equal to the angle of reflection. The SH wave is polarised perpendicular to the surface of the paper. (*d*) TR mode consists of an incident SV wave with angle of incidence $\theta_{SV}$ and reflected SV and P waves when the angle of incidence $\theta_{SV}$ exceeds the critical angle $\theta_c$ and the angle of reflection for the P wave is 90°.

are reflected from the surface. This longitudinal P wave is totally reflected by the surface as shown in figure 1(*d*). The TR mode will occur when the angle of incidence for the SV wave $\theta_{SV}$ is larger than the critical angle $\theta_c$ in which the angle of reflection for the P wave is just 90°.

In our present paper, we wish to investigate the amplification characteristics of these eigenmode acoustic waves by the conduction electrons confined in a bismuth film using a quantum-mechanical treatment in the gigahertz region such that $ql > 1$, where $q$ is the wavenumber of the acoustic waves and $l$ is the mean free path of electrons. The interaction of elastic surface waves with conduction electrons is dominated by the deformation-potential coupling in solids. The effect of energy bands on the amplification of Rayleigh waves in thin bismuth films has been studied using the Born approximation in our previous work (Wu and Tsai 1989). It was shown that the amplification coefficient of Rayleigh waves in thin bismuth films depends on the sound frequency and temperature, and the NENP model in thin bismuth films does not explain very well the electronic transport properties in the gigahertz region at very low temperatures. For our present work, in order to simplify the calculations for the amplification coefficient of eigenmode acoustic waves, we make the following main assumptions:

(i) The medium is elastically isotropic and the quasi-free-electron description of conduction electrons is valid.

(ii) Several complications due to the crystal anisotropy, possible existence of an oxidised thin layer on the surface, surface roughness, and so on, are irrelevant insofar as the qualitative features of the results are concerned.

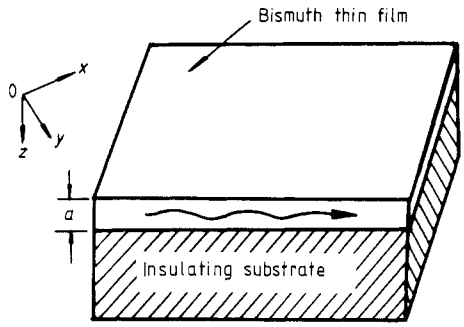


**Figure 2.** A thin layer with the thickness $a$ of a thin bismuth film and an insulating material. Acoustic waves propagate parallel to the surface of the film ($xy$ plane).

(iii) Some physical parameters have the same values as those obtained in bulk measurements.

(iv) The interaction of the surface phonons and conduction electrons is via deformation-potential coupling.

In section 2, we describe the configuration of the layered system of a semimetal and an insulator, which we shall use for determining the amplification characteristics, and specify the eigenfunctions of conduction electrons for different types of energy bands. In section 3, the quantisation of elastic eigenmode acoustic waves is presented. In section 4, we calculate the interaction between conduction electrons and eigenmode acoustic waves. In section 5, we find the amplification coefficient of eigenmode acoustic waves in thin bismuth films for different types of energy bands using the Born approximation. In section 6, some numerical results of the amplification coefficient are presented for the epitaxial layer of bismuth grown on an insulating material. Finally, we give a brief discussion of our numerical results and compare them with results for Rayleigh waves propagating in thin bismuth films.

## 2. Electronic states in a semimetal layer

The configuration of the amplifier that we consider for amplification of the eigenmode waves is shown in figure 2. A thin layer with thickness $a$ of a semimetal such as bismuth is grown epitaxially on an insulating substrate with the same elastic properties as the semimetal layer (Maissel and Glang 1970). The Cartesian coordinates are fixed so that the material occupies the half-space $z \geqslant 0$ and has the stress-free surface parallel to the $xy$ plane. In this configuration, the motion of electrons parallel to the surface may be described by plane waves and those perpendicular to the surface will be described by some kind of standing wave depending on the structure of the potential. It is assumed that the potential along the $z$ axis is a square well that has infinitely high potential barriers at $z = 0$ and $z = a$. Under this approximation, the field operator $\Psi(\boldsymbol{r})$ of conduction electrons in the second quantised form can take the form (Tamura and Sakuma 1977)

$$\Psi(\boldsymbol{r}) = S^{-1/2} \sum_{n=1}^{\infty} \sum_{k} b_{kn} \exp(\mathrm{i}\boldsymbol{k} \cdot \boldsymbol{x}) \Phi_n(z) \tag{2}$$

with

$$\Phi_n(z) = (2/a)^{1/2} \sin(n\pi z/a) \qquad n = 1, 2, 3, \ldots \tag{3}$$

where $\boldsymbol{r} = (\boldsymbol{x}, z) = (x, y, z)$, $\boldsymbol{k} = (k_x, k_y)$, $S$ is a surface area, and $b_{kn}$ and its Hermitian

conjugate $b_{kn}^{\dagger}$ are annihilation and creation operators of conduction electrons, respectively, satisfying the commutative relation of Fermi type. The energy levels of the conduction electrons $E_{kn}$ for the MNENP model of bismuth are given by the relation (Wu and Tsai 1989)

$$E_{kn}\left(1+\frac{E_{kn}}{E_g}\right)=\frac{\hbar^2k_x^2}{2m_1}+\frac{\hbar^2k_y^2}{2m_2}\left(1-\frac{n^2\pi^2\hbar^2}{2m_3a^2E_g}\right)+\frac{\hbar^4k_y^4}{4m_2^2E_g}$$
$$-\frac{\hbar^4k_x^2k_y^2}{4m_1m_2E_g}+\frac{n^2\pi^2\hbar^2}{2m_3a^2}\qquad n=1,2,3,\ldots. \tag{4}$$

Since

$$\hbar^2k_{x,\max}^2/2m_1+\hbar^2k_{y,\max}^2/2m_2+n^2\pi^2\hbar^2/2m_3a^2\simeq k_BT\ll E_g$$

for bismuth at the low temperatures in which we are interested, then equation (4) can be expanded as

$$E_{kn}\simeq-\tfrac{1}{2}E_g+\tfrac{1}{2}E_ga_n+\frac{\hbar^2k_x^2}{2m_1a_n}+\frac{\hbar^2k_y^2}{2m_2a_n^{3/2}}+\frac{\hbar^4k_y^4}{4m_2^2a_nE_g}$$
$$-\frac{\hbar^4k_x^2k_y^2}{4m_1m_2a_nE_g}\qquad n=1,2,3,\ldots \tag{5}$$

with

$$a_n=[1+(2\pi^2\hbar^2n^2)/(m_3a^2E_g)]^{1/2}. \tag{6}$$

Equation (4) can be reduced to the energy levels of electrons for the EP, ENP and NENP models of bismuth (Wu and Tsai 1989).

## 3. Quantisation of elastic eigenmode acoustic waves in thin films

The quantisation of the elastic wave field $\boldsymbol{u}(\boldsymbol{r},t)$ can be expanded in terms of the expansion coefficients, $a_J$ and $a_J^{\dagger}$, as (Ezawa 1971)

$$\boldsymbol{u}(\boldsymbol{r},t)=\sum_J\left(\frac{\hbar}{2\rho\omega_JS}\right)^{1/2}[a_J\boldsymbol{u}_J(\boldsymbol{r})\exp(-\mathrm{i}\omega_Jt)+a_J^{\dagger}\boldsymbol{u}_J^*(\boldsymbol{r})\exp(\mathrm{i}\omega_Jt)] \tag{7}$$

where $\rho$ is the mass density of the medium, $J=(\boldsymbol{q},c,m)$ is a suitable set of quantum numbers, $\boldsymbol{q}=(q_x,q_y)$ is the wavevector parallel to the surface, $c$ is the phase velocity defined by $\omega_J=c|\boldsymbol{q}|=cq$, and $m$ specifies the propagation mode of the acoustic waves. Finally, $a_J$ and its Hermitian conjugate $a_J^{\dagger}$ are the annihilation and creation operators of eigenmode acoustic waves, respectively, obeying the commutative relation of Bose type. The explicit forms of the wavefunction $\boldsymbol{u}_J(\boldsymbol{r})$ for the propagation modes P-SV, SV-P, SH and TR are given as follows (Ezawa 1971).

*3.1. P-SV mode*

$$\begin{pmatrix} u_x(r) \\ u_y(r) \\ u_z(r) \end{pmatrix} = \left(\frac{q}{2\pi}\right)^{1/2} \left[ \delta^{-1/2} \exp(-i\delta qz) \begin{pmatrix} -q_x/q \\ -q_y/q \\ \delta \end{pmatrix} + \delta^{-1/2} L \exp(i\delta qz) \begin{pmatrix} q_x/q \\ q_y/q \\ \delta \end{pmatrix} + \beta^{-1/2} K \exp(i\beta qz) \begin{pmatrix} -q_x/q \\ -q_y/q \\ 1 \end{pmatrix} \right] \exp(i\boldsymbol{q} \cdot \boldsymbol{x}) \tag{8}$$

where $\beta$, $\delta$, $K$ and $L$ are defined by the longitudinal sound velocity $c_l$, the transverse sound velocity $c_t$ and the phase velocity $c$ as

$$\beta = [(c/c_t)^2 - 1]^{1/2} \qquad \delta = [(c/c_l)^2 - 1]^{1/2}$$
$$K = \frac{4(\beta\delta)^{1/2}(\beta^2 - 1)}{(\beta^2 - 1)^2 + 4\beta\delta} \qquad L = \frac{(\beta^2 - 1)^2 - 4\beta\delta}{(\beta^2 - 1)^2 + 4\beta\delta}. \tag{9}$$

*3.2. SV-P mode*

$$\begin{pmatrix} u_x(r) \\ u_y(r) \\ u_z(r) \end{pmatrix} = i\left(\frac{q}{2\pi}\right)^{1/2} \left[ \delta^{-1/2} K \exp(i\delta qz) \begin{pmatrix} q_x/q \\ q_y/q \\ \delta \end{pmatrix} + \beta^{-1/2} \exp(-i\beta qz) \begin{pmatrix} \beta q_x/q \\ \beta q_y/q \\ 1 \end{pmatrix} + \beta^{-1/2} L \exp(i\beta qz) \begin{pmatrix} \beta q_x/q \\ \beta q_y/q \\ -1 \end{pmatrix} \right] \exp(i\boldsymbol{q} \cdot \boldsymbol{x}). \tag{10}$$

*3.3. SH mode*

$$\begin{pmatrix} u_x(r) \\ u_y(r) \\ u_z(r) \end{pmatrix} = \left(\frac{2c^2}{\pi c_t^2 \beta q}\right)^{1/2} \cos(\beta qz) \begin{pmatrix} -q_y \\ q_x \\ 0 \end{pmatrix} \exp(i\boldsymbol{q} \cdot \boldsymbol{x}). \tag{11}$$

*3.4. TR mode*

$$\begin{pmatrix} u_x(r) \\ u_y(r) \\ u_z(r) \end{pmatrix} = \left(\frac{q}{2\pi\beta}\right)^{1/2} \left[ H \exp(-\alpha qz) \begin{pmatrix} iq_x/q \\ iq_y/q \\ -\alpha \end{pmatrix} + \exp(-i\beta qz) \begin{pmatrix} i\beta q_x/q \\ i\beta q_y/q \\ i \end{pmatrix} + G \exp(i\beta qz) \begin{pmatrix} i\beta q_x/q \\ i\beta q_y/q \\ -i \end{pmatrix} \right] \exp(i\boldsymbol{q} \cdot \boldsymbol{x}) \tag{12}$$

where

$$\alpha = [1 - (c/c_l)^2]^{1/2} \qquad G = [(\beta^2 - 1)^2 - 4i\alpha\beta]/[(\beta^2 - 1)^2 + 4i\alpha\beta]$$
$$H = 4\beta(\beta^2 - 1)/[(\beta^2 - 1)^2 + 4i\alpha\beta]. \tag{13}$$

## 4. Interaction between conduction electrons and eigenmode acoustic waves

The interaction Hamiltonian between conduction electrons and eigenmode acoustic waves due to the deformation-potential coupling can be expressed in the second quantisation representation as

$$H = C\int \Psi^*(\boldsymbol{r})\nabla\cdot\boldsymbol{u}(\boldsymbol{r})\Psi(\boldsymbol{r})\,\mathrm{d}\boldsymbol{r}$$

$$= CS^{-1/2}\sum_{n,n'}\sum_{k,J}[b^{\dagger}_{k+q,n'}b_{k,n}a_J\Delta^J_{n'n} + (\text{Hermitian conjugate})] \tag{14}$$

where $C$ is the deformation potential. The function $\Delta^J_{n'n}$ for each mode is given as follows.

### 4.1. *P-SV mode*

$$\Delta^J_{n'n} = -\mathrm{i}\left(\frac{\hbar}{4\pi\rho\delta c}\right)^{1/2}\left(\frac{c}{c_1}\right)^2 q\int_0^a \Phi^*_{n'}(z)[\exp(-\mathrm{i}\delta qz) - L\exp(\mathrm{i}\delta qz)]\Phi_n(z)\,\mathrm{d}z. \tag{15}$$

### 4.2. *SV-P mode*

$$\Delta^J_{n'n} = -\left(\frac{\hbar}{4\pi\rho\delta c}\right)^{1/2}\left(\frac{c}{c_1}\right)^2 qK\int_0^a \Phi^*_{n'}(z)\exp(\mathrm{i}\delta qz)\Phi_n(z)\,\mathrm{d}z. \tag{16}$$

### 4.3. *SH mode*

$$\Delta^J_{n'n} = 0. \tag{17}$$

### 4.4. *TR mode*

$$\Delta^J_{n'n} = -\left(\frac{\hbar}{4\pi\rho\beta c}\right)^{1/2}\left(\frac{c}{c_1}\right)^2 qH\int_0^a \Phi^*_{n'}(z)\exp(-\alpha qz)\Phi_n(z)\,\mathrm{d}z. \tag{18}$$

From equation (17), it can be seen that no interaction of conduction electrons and SH mode acoustic waves occurs in semimetals such as bismuth.

## 5. Amplification coefficient of eigenmode acoustic waves

It is known that conduction electrons never travel freely in semimetals, but are scattered by a variety of sources before and after they emit or absorb the phonons we should observe. The induced electric field due to the deformation-potential coupling can cause the screening of the electron–phonon interaction in semimetals. Using the Hamiltonian

in equation (14) and neglecting vertex corrections other than the screening effect of the electrons, the width $\Gamma^{(J)}$ of the eigenmode wave can be expressed by

$$\Gamma^{(J)}(\hbar\omega_J) = 2\sum_{n,n'}[C(q)]^2|\Delta^J_{n'n}|^2\int\frac{d\boldsymbol{k}}{(2\pi)^2}\int\frac{d\varepsilon}{2\pi}[f(\varepsilon-\hbar\omega_J)-f(\varepsilon)] \times A_n(\boldsymbol{k},\varepsilon)A_{n'}(\boldsymbol{k}-\boldsymbol{q},\varepsilon-\hbar\omega_J) \tag{19}$$

where

$$C(q) = C/\varepsilon_1(q) \qquad \varepsilon_1 = 1 + 6\pi^2 N c_l^2/\varepsilon_0 q^2 c^2 E_F$$

$\varepsilon_0$ is the static dielectric constant, $N$ is the electron concentration and $E_F$ is the Fermi energy. The Fermi–Dirac distribution function is

$$f(\varepsilon) = \{\exp[(\varepsilon - E_F)/k_B T] + 1\}^{-1}$$

and $A_n(\boldsymbol{k},\varepsilon)$ is the spectral function of the one-electron Green function with the quantised level $n$ of conduction electrons. In the first approximation, we employ the Born approximation and then simply replace the spectral function by the $\delta$ function,

$$A_n(\boldsymbol{k},\varepsilon) = 2\pi\delta(\varepsilon - E_{kn}). \tag{20}$$

In a situation where conduction electrons have a drift velocity $\boldsymbol{v}$ in the direction of the acoustic wavevector $\boldsymbol{q}$, we have to replace $\hbar\omega_J$ by $-\hbar\omega_J x$ with the drift parameter $x = |\boldsymbol{v}|/c - 1$. Then

$$f(\varepsilon - \hbar\omega_J) - f(\varepsilon) = -(\hbar\omega_J x/4k_B T)\,\mathrm{sech}^2[(\varepsilon - E_F)/2k_B T]. \tag{21}$$

From equations (19)–(21), the amplification coefficient $\alpha^J$ of eigenmode acoustic waves can be obtained as (Landau and Lifshitz 1977)

$$\alpha^J = -\frac{\Gamma^J_{\mathrm{Born}}(-\hbar\omega_J x)}{\hbar c}$$

$$= \frac{\omega_J x}{4\pi c k_B T}\sum_{i,j}[C(q)]^2|\Delta^J_{ij}|^2\int d\boldsymbol{k}\int d\varepsilon\,\mathrm{sech}^2[(\varepsilon - E_F)/2k_B T] \times \delta(\varepsilon - E_{ki})\delta(\varepsilon + \hbar\omega_J x - E_{k-q,j}). \tag{22}$$

Using the eigenvalues for energy bands of bismuth, we can obtain the more explicit expression for $\alpha^J$ as given in appendix 1. If we take the directions of the wavevector $\boldsymbol{q}$ in [1 1 0] crystal axis, the function $|\Delta^J_{ij}|^2$ for each mode is given in appendix 2. From these one can obtain numerical results as shown in the next section.

## 6. Numerical results and discussion

The relevant values of physical parameters for bismuth are (Harrison 1960, Smith *et al* 1964, Fal'kovskiĭ 1968, Fukami *et al* 1979): $m_1 = m_0/172$, $m_2 = m_0/0.8$, $m_3 = m_0/88.5$ ($m_0$ is the free-electron mass), $\rho = 9.8\,\mathrm{g\,cm^{-3}}$, $N = 2.75\times10^{17}\,\mathrm{cm^{-3}}$, $\varepsilon_0 = 10$, $c_l = 4.9\times10^5\,\mathrm{cm\,s^{-1}}$, $c_t = 3.8\times10^5\,\mathrm{cm\,s^{-1}}$, $E_g = 0.0153\,\mathrm{eV}$, $E_F = 0.0276\,\mathrm{eV}$, $C = 10\,\mathrm{eV}$ and $a = 1\,\mu\mathrm{m}$. Since $|\Delta^J_{ij}|^2 = 0$ for the SH mode waves, the amplification coefficient is zero for any frequency and electric field. Thus we do not discuss the amplification coefficient of SH mode waves in bismuth films.

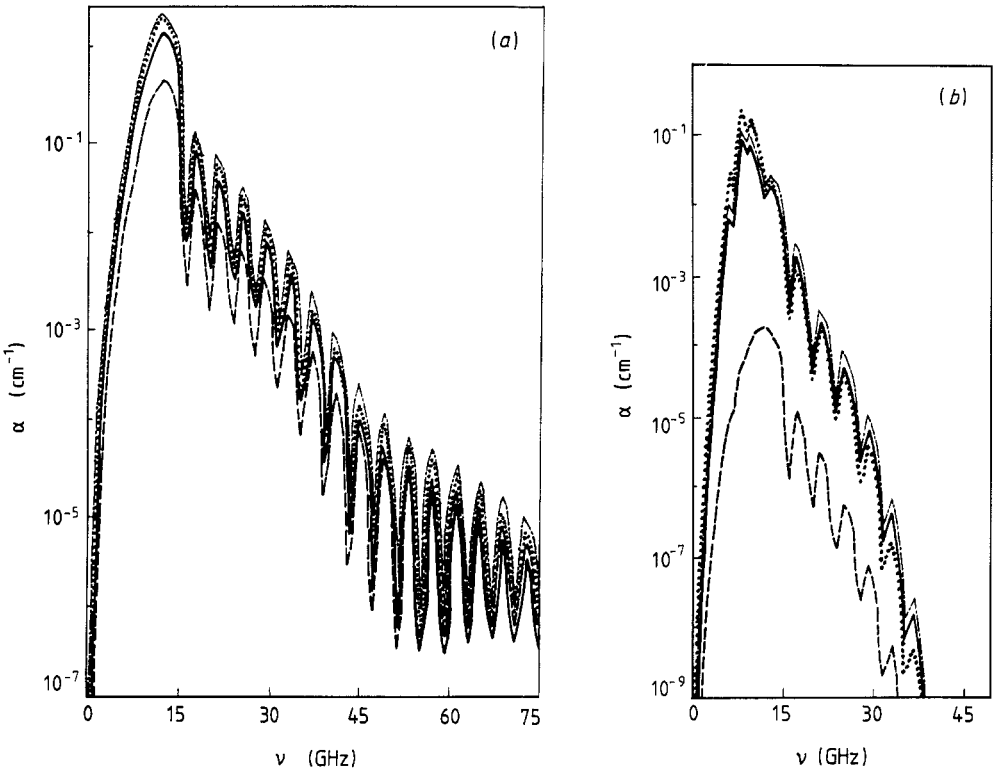


**Figure 3.** Amplification coefficient of acoustic waves for P-SV mode as a function of frequency in bismuth films with $x = 100$ ($E = 2\ \mathrm{V\ cm^{-1}}$) at (*a*) $T = 77$ K and (*b*) $T = 4.2$ K: (———) MNENP model; (– – –) NENP model; (–·–·–) ENP model; (· · · ·) EP model.

### 6.1. *P-SV mode waves*

In this configuration, we consider a situation in which the reflected P and SV waves are generated with the angle of incidence $\theta_P = 54.74°$; then $\tan\theta_P = \delta^{-1} = \sqrt{2}$. In this case, the phase velocity $c$ is equal to $(\sqrt{6}/2)c_l$ and the wavevector $\boldsymbol{q}$ is parallel to the [110] axis. The frequency ($\nu = \omega_J/2\pi$) dependence of the amplification coefficient at $x = 100$ ($E = 2\ \mathrm{V\ cm^{-1}}$) is shown in figure 3. It shows that the amplification coefficient increases rapidly with frequency up to around $\nu = 11$ GHz and then drops off and oscillates with frequency. In figure 3(*a*) for a temperature of 77 K, it can be seen that the amplification coefficient for the MNENP model is close to those for the ENP and EP models in the frequency region $\nu < 55$ GHz, while in the high-frequency region $\nu > 55$ GHz the amplification coefficient for the NENP model is close to those for the ENP and EP models. The oscillations of the amplification coefficient with the frequency of acoustic waves are different from the results for Rayleigh waves propagating in thin bismuth films (Wu and Tsai 1989). For a temperature of 4.2 K as shown in figure 3(*b*), the amplification coefficient decreases more rapidly with frequency than that for a temperature of 77 K after passing the principal maximum point. Moreover, the difference between the amplification coefficient of the NENP model and those of the EP, ENP and MNENP models becomes larger. Figure 4 shows the amplification coefficients versus the drift parameter

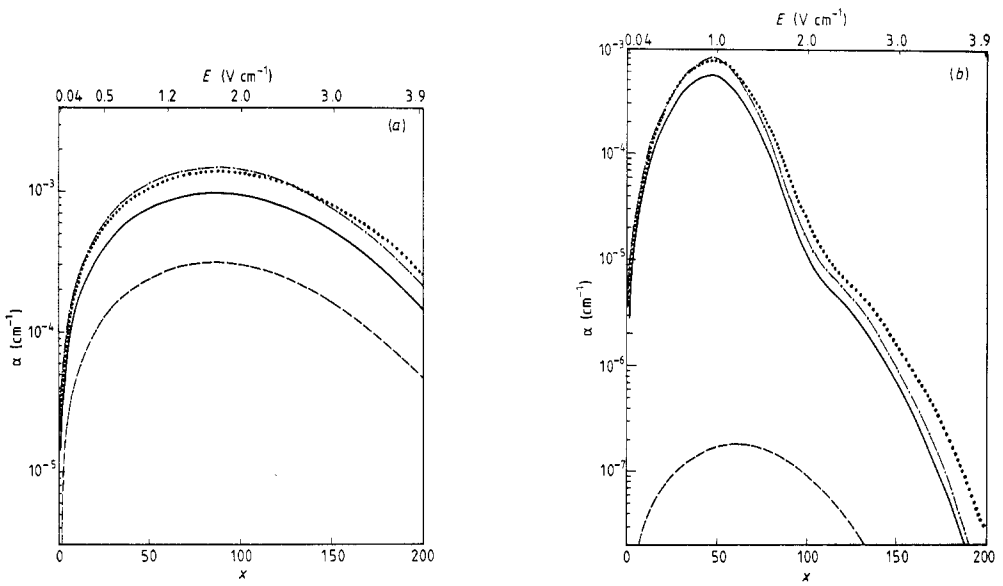


**Figure 4.** Amplification coefficient of acoustic waves for P-SV mode versus drift parameter $x$ or applied electric field $E$ in bismuth films with $\nu = 3$ GHz at (*a*) $T = 77$ K and (*b*) $T = 4.2$ K: (———) MNENP model; (– – –) NENP model; ((– · – · –) ENP model; (· · · ·) EP model.

$x$ (or the applied electric field $E$) with the frequency $\nu = 3$ GHz. In figure 4(*a*) for $T =$ 77 K, it can be seen that the amplification coefficient increases with the drift parameter $x$ and then decreases monotonically. It can also be seen that the amplification coefficient for the MNENP model lies between those for the NENP model and the EP or ENP model. However, when the temperature decreases to 4.2 K as shown in figure 4(*b*), the amplification for the EP, ENP and MNENP models increases rapidly to a maximum point and then decreases rapidly with the drift parameter $x$. Moreover, there exists an inflection point in the amplification coefficient for the EP, ENP and MNENP models, but the amplification coefficient for the NENP model appears to change monotonically with the drift parameter or the electric field. The deviation of the amplification coefficient for the NENP model from those for the EP, ENP and MNENP models becomes very large with decreasing temperature.

### 6.2. *SV-P mode waves*

Consider a situation in which the reflected SV and P waves are generated with the angle of incidence $\theta_{SV} = 35.2°$ ($\tan\theta_{SV} = \beta^{-1} = 1/\sqrt{2}$). In this case, the phase velocity $c$ is equal to $\sqrt{3}c_t$ and the wavevector $\boldsymbol{q}$ is also parallel to the [1 1 0] axis. The frequency dependence of the amplification coefficient at $x = 100$ ($E = 2.2$ V cm$^{-1}$) is shown in figure 5. In figure 5(*a*) for $T = 77$ K, it is found that the amplification coefficient increases rapidly with frequency up to about $\nu = 25$ GHz and then decreases and oscillates with frequency. This phenomenon of oscillations with the frequency of acoustic waves is also different from that of Rayleigh waves (Wu and Tsai 1989). It can be seen that when the frequency is larger than 53 GHz, the amplification coefficient for the NENP model becomes closer than that for the MNENP model to those for the EP and ENP models. As

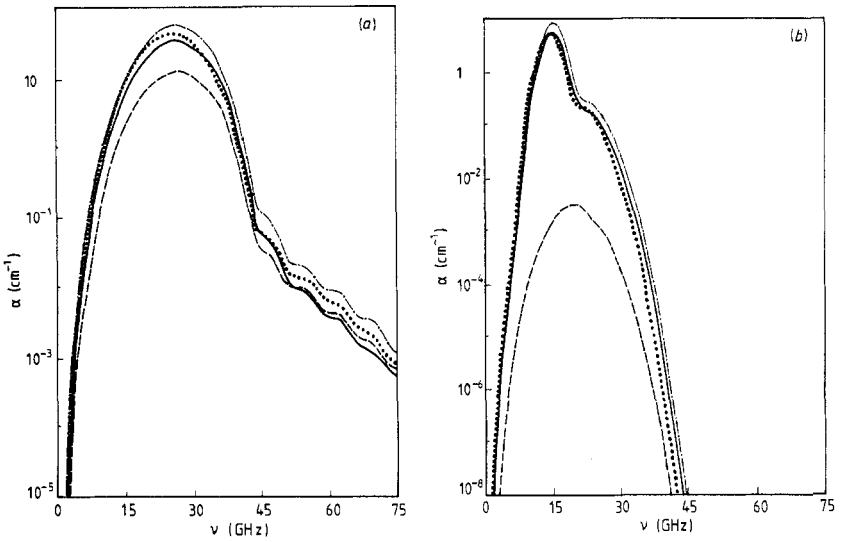


**Figure 5.** Amplification coefficient of acoustic waves for SV-P mode as a function of frequency in bismuth films with $x = 100$ ($E = 2.2$ V cm$^{-1}$) at (*a*) $T = 77$ K and (*b*) $T = 4.2$ K: (———) MNENP model; (– – –) NENP model; (– · – · –) ENP model; (· · · ·) EP model.

the temperature decreases to $T = 4.2$ K as shown in figure 5(*b*), no oscillations of the amplification coefficient can be observed. It can also be seen that the inflection point in the amplification coefficient for the NENP model disappears. Moreover, the difference between the amplification coefficient of the NENP model and those of the EP, ENP and MNENP models becomes larger in the intermediate-frequency region. We plot the amplification coefficients versus the drift parameter $x$ (or the applied electric field $E$) with the frequency $\nu = 3$ GHz as shown in figure 6. In figure 6(*a*) for a temperature of $T = 77$ K, it is shown that the amplification coefficient increases with the drift parameter and then decreases monotonically. It can also be seen that the amplification coefficient for the MNENP model lies between those for the NENP model and the EP or ENP model. As the temperature decreases to $T = 4.2$ K as shown in figure 6(*b*), it can be seen that the difference of the amplification coefficient for the NENP model and those for the EP, ENP, or MNENP model becomes quite large.

### 6.3. TR mode waves

The frequency dependence of the amplification coefficient at $x = 100$ ($E = 1.42$ V cm$^{-1}$) is plotted as shown in figure 7. In figure 7(*a*), it can be seen that the amplification coefficient increases with frequency up to around $\nu = 24$ GHz and then decreases with increasing frequency at $T = 77$ K. The inflection point of the amplification coefficient can be observed. However, as the temperature decreases to $T = 4.2$ K as shown in figure 7(*b*), the inflection point of the amplification coefficient for the NENP model disappears. This result is the same as that for Rayleigh waves (Wu and Tsai 1989). Figure 8 shows the amplification coefficient versus the drift parameter $x$ (or the applied electric field $E$) with $\nu = 3$ GHz. In figure 8(*a*) for a temperature of 77 K, it can be seen that the amplification coefficient increases with the drift parameter up to $x = 70$ ($E = 1$ V cm$^{-1}$)

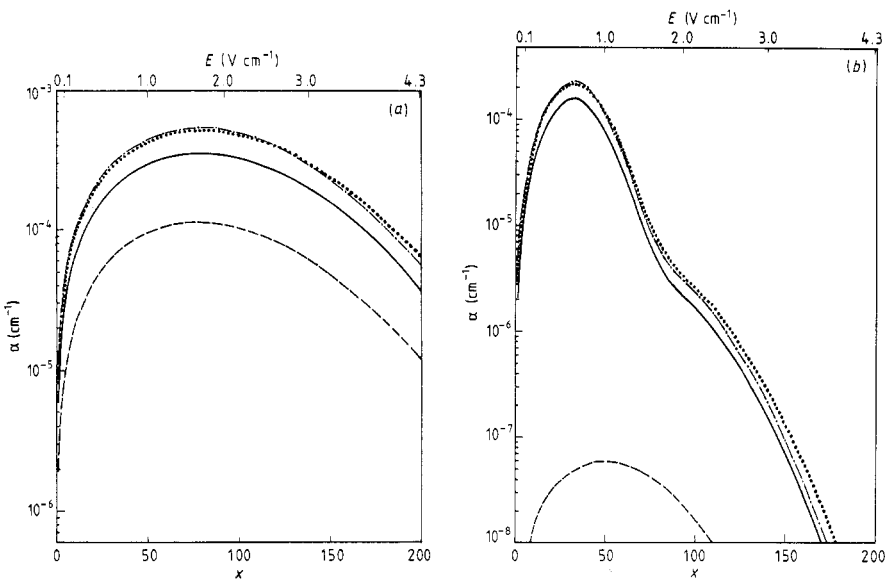


**Figure 6.** Amplification coefficient of acoustic waves for SV-P mode versus drift parameter $x$ or applied electric field $E$ in bismuth films with $\nu = 3$ GHz at (*a*) $T = 77$ K and (*b*) $T = 4.2$ K: (———) MNENP model; (– – –) NENP model; (– · – · –) ENP model; (· · · ·) EP model.

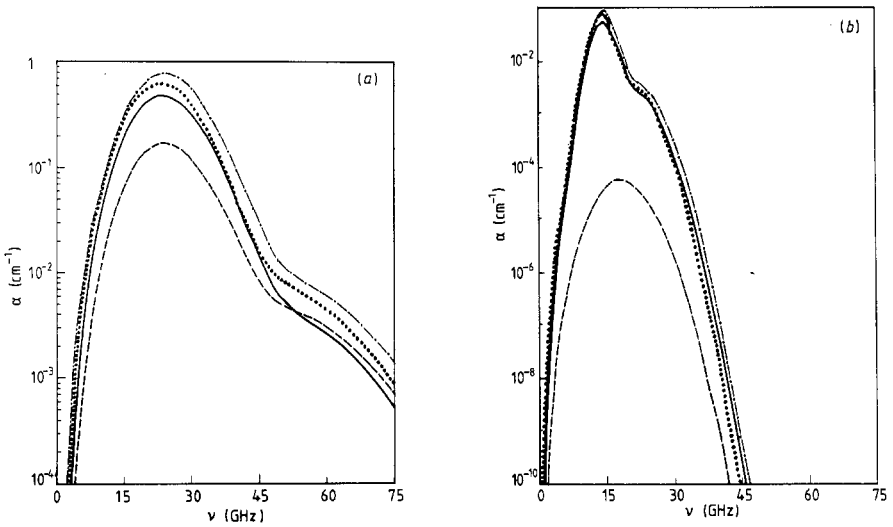


**Figure 7.** Amplification coefficient of acoustic waves for TR mode as a function of frequency in bismuth films with $x = 100$ ($E = 1.42$ V cm$^{-1}$) at (*a*) $T = 77$ K and (*b*) $T = 4.2$ K: (———) MNENP model; (– – –) NENP model; (– · – · –) ENP model; (· · · ·) EP model.

and then decreases monotonically with the drift parameter. For the temperature at $T =$ 4.2 K as shown in figure 8(*b*), we can see that the maximum point is shifted to around $x = 30$ ($E = 0.44$ V cm$^{-1}$) for the EP, ENP and MNENP models, while for the NENP model the

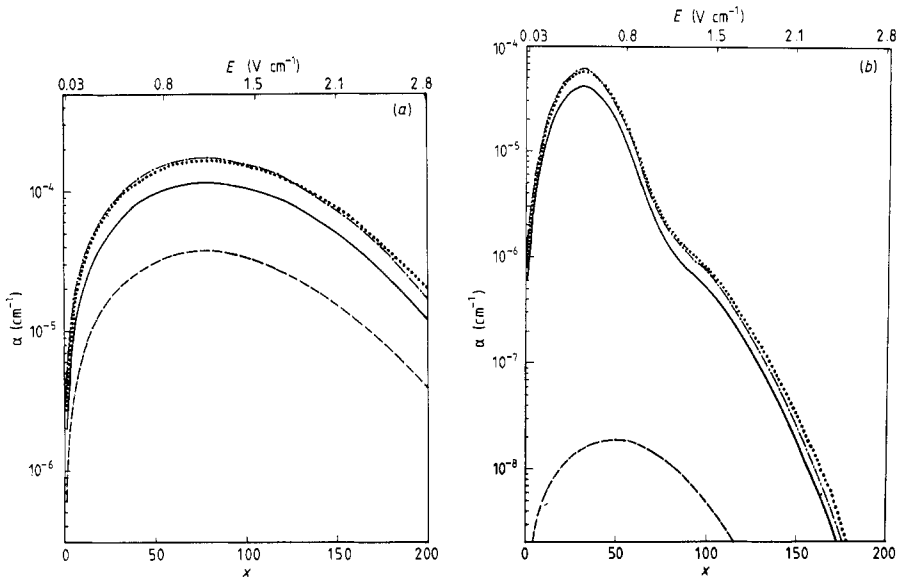


**Figure 8.** Amplification coefficient of acoustic waves for TR mode versus drift parameter $x$ or applied electric field $E$ in bismuth films with $\nu = 3$ GHz at (*a*) $T = 77$ K and (*b*) $T = 4.2$ K: (———) MNENP model; (– – –) NENP model; (– · – · –) ENP model; (· · · ·) EP model.

maximum point is at $x = 50$ ($E = 0.72$ V cm$^{-1}$). The inflection point in the amplification coefficient for the NENP model disappears and the difference between the amplification coefficient for the NENP model and those for the EP, ENP and MNENP models becomes large at low temperatures.

## 7. Conclusions

The amplification coefficient for the eigenmode acoustic waves in thin bismuth films has been calculated using the Born approximation, which is valid in the region $\omega_J\tau > 1$ with $\tau = 2 \times 10^{-10}$ s (Fal'kovskiĭ 1968). We investigate the effect of energy bands on the amplification of surface phonons in thin bismuth films, neglecting the effect of the relaxation time of electrons. From our present calculations presented here, it shows that the amplification coefficient in bismuth films for the MNENP model is close to those for the EP and ENP models, and the amplification coefficient for the NENP model deviates from those for the EP, ENP and MNENP models at low temperatures. Comparing equation (1*c*) with equation (1*d*), it can be seen that the correction term $p_y^4/4m_2m_2'E_g$ in the NENP model causes the over-correction as the temperature decreases to low temperatures. However, some extra correction terms $-p_x^2p_y^2/4m_1m_2E_g$ and $-p_y^2p_z^2/4m_2m_3E_g$ in the MNENP model will compensate the over-correction in the NENP model. Consequently, the NENP model of bismuth could not be used satisfactorily to explain the interaction of conduction electrons and surface phonons in the low-temperature region.

It has been found that the amplification coefficient of the eigenmode acoustic waves depends strongly upon the temperature. From equation (22) and appendix 1, it can be shown that the amplification coefficient is roughly proportional to $T^{-1/2}\exp[-F(n, n')/$

$T]$, where $F(n, n')$ is independent of temperature. This temperature-dependent factor comes from the energy-band structure of solids. Consequently, the temperature dependence of the amplification coefficient arises from the energy-band structure in solids. Moreover, some oscillations can be observed in the higher-frequency region for the P-SV and SV-P mode waves. These oscillations come from the contribution of the function $|\Delta^J_{nn'}|^2$, which contains harmonic functions of the frequency, $\cos(\pi A)$ and $\sin(\pi A)$, due to the relation $A = \delta qa/\pi = 2\delta a\nu/c$. From appendix 2, it can be seen that the oscillations for the P-SV mode waves are manifest much more considerably than those for the SV-P mode waves. Moreover, as the temperature decreases, these oscillations will be diminished, or even vanish, as shown in figure 5($b$) for the SV-P mode waves. From equation (22) (or more explicit expressions shown in appendix 1) and expressions for $|\Delta^J_{ij}|^2$ shown in appendix 2, it can be seen that the amplification coefficient as a function of drift parameter $x$ is dominated by the factor

$$f(x) = x\{\exp[C_1(x - C_2)^2 - C_3(i, j)(x - C_4)]\} \tag{23}$$

where $C_1$, $C_2$, $C_3(i, j)$ and $C_4$ are independent of $x$. It can be shown that there exist at most two local extrema in equation (23). These extrema depend on the quantum numbers $i$ and $j$. In our numerical results, as shown in figures 4, 6 and 8, only one maximum point can be observed; the second extremum point could have degenerated to an inflection point at low temperatures for the EP, ENP and MNENP models. Therefore, the amplification coefficient depends on the energy bands of solids, the temperature, the frequency of eigenmode waves and the applied electric field. At low temperatures, the quantum effect becomes important, which is valid when $ql > 1$ or $\omega_J\tau > 1$ in our present calculations. We may disregard all defects and consider a thin film of an ideal solid with perfectly parallel boundary planes. Thus the scattering of surface irregularities (Steg and Klemens 1970, Sakuma 1972) can be neglected at low temperatures.

**Acknowledgment**

The authors wish to acknowledge the partial financial support from the National Science Council of China in Taiwan.

## Appendix 1. Explicit forms of $\alpha_J$

*A1.1. EP model*

$$\alpha^J = \left(\frac{2}{\pi}\right)^{1/2}\left(\frac{x}{\hbar^3}\right)m_1\left(\frac{m_2}{k_B T}\right)^{1/2}[C(q)]^2\sum_{n=1}^{\infty}(-1)^{n+1}n^{1/2}\exp[nP(q)/k_B T]$$
$$\times\sum_i\sum_j\{\exp[-nQ(q; i, j)/k_B T]\}|\Delta^J_{ij}|^2 \tag{A1}$$

where

$$[C(q)]^2 = C^2\left(1 + \frac{6\pi e^2 N c_1^2}{\varepsilon_0\omega_J^2 E_F}\right)^{-2} \tag{A2}$$

$$P(q) = E_F - (m_1/2q^2\hbar^2)[\hbar\omega_J x - (q\hbar)^2/2m_1]^2 \tag{A3}$$

and

$$Q(q;i,j)=\frac{\pi^2\hbar^2 i^2}{2m_3a^2}+\frac{m_1}{2q^2\hbar^2}\left[\frac{\pi^2\hbar^2}{m_3a^2}\left(\hbar\omega_J x-\frac{q^2\hbar^2}{2m_1}\right)(i^2-j^2)+\frac{\pi^4\hbar^4}{4m_3^2a^4}(i^2-j^2)^2\right]. \tag{A4}$$

*A1.2. ENP model*

$$\alpha^J=\left(\frac{2}{\pi}\right)^{1/2}\left(\frac{x}{\hbar^3}\right)m_1\left(\frac{m_2}{k_BT}\right)^{1/2}[C(q)]^2\sum_{n=1}^{\infty}(-1)^{n+1}n^{1/2}\exp[n(\tfrac{1}{2}E_g+E_F)/k_BT]$$

$$\times\sum_i\sum_j a_i^{1/2}a_j\{\exp[-nE_gR(q;i,j)/2k_BT]\}|\Delta_{ij}^J|^2 \tag{A5}$$

where

$$R(q;i,j)=a_i+\frac{m_1E_ga_j^2}{q^2\hbar^2a_i}\left(\frac{\hbar\omega_J x}{E_g}-\frac{q^2\hbar^2}{2m_1E_ga_j}+\tfrac{1}{2}(a_i-a_j)\right)^2. \tag{A6}$$

*A1.3. NENP model*

$$\alpha^J=\left(\frac{1}{\sqrt{2\pi}}\right)\left(\frac{x}{\hbar^3}\right)m_1\frac{(m_2E_g)^{1/2}}{k_BT}[C(q)]^2\sum_{n=1}^{\infty}(-1)^{n+1}n\exp[n(\tfrac{1}{2}E_g+E_F)/k_BT]$$

$$\times\sum_i\sum_j a_jK_{1/4}\left(\frac{nE_g}{8a_ik_BT}\right)\{\exp[-nE_gR(q;i,j)/2k_BT]\}|\Delta_{ij}^J|^2 \tag{A7}$$

where $K_\nu(z)$ is the modified Bessel function of order $\nu$ (Abramowitz and Stegun 1964, Gradshteyn and Ryzhik 1965).

*A1.4. MNENP model*

$$\alpha^J=\left(\frac{1}{\pi}\right)\left(\frac{x}{\hbar^3}\right)\frac{(m_1^2m_2E_g)^{1/2}}{k_BT}[C(q)]^2\sum_{n=1}^{\infty}(-1)^{n+1}n\exp[n(\tfrac{1}{2}E_g+E_F)/k_BT]$$

$$\times\sum_i\sum_j a_i^{1/2}a_j\left(\frac{S(q;i,j)}{T(q;i,j)}\right)^{1/2}K_{1/4}\left[\left(\frac{nE_g}{2k_BT}\right)\frac{S^2(q;i,j)}{T(q;i,j)}\right]|\Delta_{ij}^J|^2$$

$$\times\exp\left[-\left(\frac{nE_g}{2k_BT}\right)\left(R(q;i,j)-\frac{S^2(q;i,j)}{T(q;i,j)}\right)\right] \tag{A8}$$

where

$$S(q;i,j)=2a_i^{-1/2}+a_i^2+q\hbar a_i^{1/2}(m_1E_g)^{-1/2}[R(q;i,j)-a_i]^{1/2}-a_iR(q;i,j) \tag{A9}$$

and

$$T(q;i,j)=16a_i+2q^2\hbar^2a_i/m_1E_g-8q\hbar a_i^{3/2}(m_1E_g)^{-1/2}[R(q;i,j)-a_i]^{1/2}. \tag{A10}$$

## Appendix 2. Explicit forms of $|\Delta_{ij}^J|^2$

*A2.1. P-SV mode*

$$|\Delta_{ij}^J|^2 = \left(\frac{8q^2\hbar}{\pi^3\rho\delta c}\right)\left(\frac{c}{c_1}\right)^4 A^2(1+D)^2 i^2 j^2 \times \frac{1-(-1)^{i+j}\cos(\pi A) - 2D(1+D)^{-2}\sin^2(\pi A)}{[(i-j)^2 - A^2]^2[(i+j)^2 - A^2]^2} \tag{A11}$$

where

$$A = \delta q a/\pi \tag{A12}$$

and

$$D = \frac{(\beta^2-1)^2 - 4\beta\delta}{(\beta^2-1)^2 + 4\beta\delta}. \tag{A13}$$

*A2.2. SV-P mode*

$$|\Delta_{ij}^J|^2 = \left(\frac{8q^2\hbar}{\pi^3\rho\delta c}\right)\left(\frac{c}{c_1}\right)^4 A^2 B^2 i^2 j^2 \frac{1-(-1)^{i+j}\cos(\pi A)}{[(i-j)^2 - A^2]^2[(i+j)^2 - A^2]^2} \tag{A14}$$

where

$$B = \frac{4(\beta\delta)^{1/2}(\beta^2-1)}{(\beta^2-1)^2 + 4\beta\delta}. \tag{A15}$$

*A2.3. SH mode*

$$|\Delta_{ij}^J|^2 = 0. \tag{A16}$$

*A2.4. TR mode*

$$|\Delta_{ij}^J|^2 = \left(\frac{64q^2\hbar}{\pi^3\rho c}\right)\left(\frac{c}{c_1}\right)^4 \frac{(A')^2\beta(\beta^2-1)^2 i^2 j^2[1-(-1)^{i+j}\exp(-\pi A')]^2}{[(\beta^2-1)^4 + 16\alpha^2\beta^2][(i-j)^2 + (A')^2]^2[(i+j)^2 + (A')^2]^2} \tag{A17}$$

where

$$A' = \alpha q a/\pi. \tag{A18}$$

## References

Abramowitz M and Stegun I A 1964 *Handbook of Mathematical Functions* (Washington DC: National Bureau of Standards)
Cohen M H 1961 *Phys. Rev.* **121** 387–95
Dinger R J and Lawson A W 1970 *Phys. Rev.* B **1** 2418–23
—— 1971 *Phys. Rev.* B **3** 253–62
—— 1973 *Phys. Rev.* B **7** 5215–27
Ezawa H 1971 *Ann. Phys., NY* **67** 438–60

Fal'kovskiĭ L A 1968 *Usp. Fiz. Nauk* **94** 3–41 (Engl. Transl. 1969 *Sov. Phys.–Usp.* **11** 1–21)
Fukami T, Yamaguchi T and Mass S 1979 *J. Phys. Soc. Japan* **47** 423–34
Gradshteyn I S and Ryzhik I M 1965 *Table of Integrals, Series and Products* (New York: Academic)
Grishin A M and Kaner E A 1972 *Zh. Eksp. Teor. Fiz.* **63** 2304–15 (Engl. transl. 1973 *Sov. Phys.–JETP* **36** 1217–22)
Harrison M J 1960 *Phys. Rev.* **119** 1260–9
Koch J F and Jensen J D 1969 *Phys. Rev.* **184** 643–54
Landau L D and Lifshitz 1977 *Quantum Mechanics–Nonrelativistic Theory* (Oxford: Pergamon)
Lax B 1958 *Rev. Mod. Phys.* **30** 122–54
McClure J W and Choi K H 1977 *Solid State Commun.* **21** 1015–18
Maissel L I and Glang R 1970 *Handbook of Thin Films Technology* (New York: McGraw-Hill)
Maltz M and Dresselhaus M S 1970 *Phys. Rev.* B **2** 2877–87
Michenaud J P, Heremans J, Boxus J and Haumont C 1981 *J. Phys. C: Solid State Phys.* **14** L13–16
Michenaud J P, Heremans J, Shayegan M and Haumont C 1982 *Phys. Rev.* B **26** 2552–9
Sakuma T 1972 *Phys. Rev. Lett.* **29** 1394–6
Shoenberg D 1957 *Progress in Low Temperature Physics* vol 2 (New York: Interscience) ch 8
Smith G E, Baraff G A and Rowell J M 1964 *Phys. Rev.* **135** A1118–24
Steg P G and Klemens P G 1970 *Phys. Rev. Lett.* **24** 381–3
Tamura S and Sakuma T 1977 *Phys. Rev.* B **15** 4948–54
Vecchi M P, Pereira J R and Dresselhaus M S 1976 *Phys. Rev.* B **14** 298–317
Wu C C and Tsai J 1989 *J. Phys.: Condens. Matter* **1** 2851–5